Instability suppression in viscoelastic film flows down an inclined plane lined with a deformable solid layer

Aashish Jain and V. Shankar*
Department of Chemical Engineering, Indian Institute of Technology, Kanpur 208 016, India
(Received 26 June 2007; published 23 October 2007)

The linear stability of viscoelastic (Oldroyd-B) film flow down an inclined plane lined with a deformable (neo-Hookean) solid layer is analyzed using low-wave-number asymptotic analysis and the Chebyshev-Tau spectral numerical method. The free surface of film flows of viscoelastic liquids, unlike that of their Newtonian counterparts, becomes unstable in flow down a rigid inclined surface even in the absence of fluid inertia, due to the elastic nature of the liquids. For film flow past a deformable solid, our low-wave-number asymptotic analysis reveals that the solid deformability has a stabilizing effect on the free-surface instability, and, remarkably, this prediction is insensitive to rheology of the liquid film, be it viscoelastic or Newtonian. Using the spectral numerical method, we demonstrate that the free-surface instability can be completely suppressed at all wave numbers when the solid becomes sufficiently deformable. For the case of pure polymeric liquids without any solvent, when the solid layer is made further deformable, both the free surface and the liquid-solid interface are destabilized at finite wave numbers. We also demonstrate a type of mode exchange phenomenon between the modes corresponding to the two interfaces. Importantly, our numerical results show that there is a sufficient range of shear modulus of the solid where both the modes are stable at all wave numbers. For polymer solutions described by the Oldroyd-B model, while the free-surface instability is suppressed by the deformable solid, a host of new unstable modes appear at finite Reynolds number and wave number because of the coupling between liquid flow and free shear waves in the solid. Our study thus demonstrates that the elastohydrodynamic coupling between liquid flow and solid deformation can be exploited either to suppress the free-surface instability (present otherwise in rigid inclines) in viscoelastic film flows, or to induce new instabilities that are absent in flow adjacent to rigid surfaces.

DOI: 10.1103/PhysRevE.76.046314 PACS number(s): 47.20.−k

I. INTRODUCTION

Gravity-driven film flows with free surfaces of both Newtonian and rheologically complex liquids are frequently encountered in a diverse class of physical settings and technological applications such as precision coating in photographic films, flow in lung airways involving liquid linings, etc. A ubiquitous feature of liquid film flows past a solid wall is the instability [1–7] of the free surface, which manifests as gravity-driven surface waves with wavelengths much larger than the film thickness. From a fundamental standpoint, the motivation for studying these systems stems from the rich spatiotemporal nonlinear dynamics exhibited by these film flows (e.g., solitary waves, transitions from laminar to more complex and turbulent flows), and for this reason these flows have served as model systems in the understanding of instability and bifurcation phenomena [8]. Even from a technological perspective, there is immense interest in the understanding, prediction, and control of free-surface instabilities in coating operations [9], where stable film flows of single or multiple layers are desirable because the occurrence of instabilities in the free surface is detrimental to the quality of the manufactured coating product. With a view to controlling and suppressing the free-surface instability, several strategies have been explored in the literature, including in-plane oscillations of the bottom wall [10–14], wall heating [15], and the presence of surfactants at the free surface [16–19]. Recently, soft solid coatings were suggested as potential candidates to suppress free-surface instabilities in Newtonian liquid flows [20,21]. These studies showed that, when the solid layer becomes sufficiently deformable, the elastohydrodynamic coupling between the liquid flow and solid deformation suppresses the free-surface instability for perturbations with any wavelength, without introducing any additional instability in the system. However, many applications in coating processes involve polymeric liquids, which are viscoelastic. The viscoelastic nature of polymeric liquids significantly alters the stability and dynamics of film flows, and it renders the free surface unstable even in the absence of fluid inertia [4–7]. In view of this alternative destabilizing mechanism in polymeric films involving elastic effects, the question arises as to whether the previous predictions of instability suppression for Newtonian liquid flows are still valid for viscoelastic films. In particular, is there a generic mechanism whereby the free-surface instability in film flows is suppressed by deformable solid coatings, irrespective of the fluid rheology? To address this question, we undertake here a comprehensive study of gravity-driven viscoelastic film flow past a deformable solid layer using both an analytical long-wave asymptotic technique and a numerical spectral solution. Before proceeding to formulate the problem, we first review relevant literature in this area, and motivate the context for the present study.

The linear instability of the free surface of Newtonian film flows down an inclined plane was first demonstrated by Benjamin [1] and Yih [2]. Yih used a long-wave analysis and

*Author to whom correspondence should be addressed; vshankar@iitk.ac.in

showed that film flow is unstable at any nonzero Reynolds number for rigid vertical inclines. For surfaces inclined at an angle, a finite nonzero critical Reynolds number is required for the instability. In stark contrast, a series of studies [4–7] carried out for polymeric liquids, which are viscoelastic in nature, showed that the film flow is unstable even at zero Reynolds number (i.e., creeping flow), but at nonzero Weissenberg number, which is a nondimensional number characterizing the relaxation time or elasticity in the liquid. Clearly, the noninertial destabilizing mechanism in viscoelastic liquids is qualitatively different from that for Newtonian liquids, and this elastically driven free-surface instability was attributed to the coupling between the base flow and perturbation velocity and stresses at the free surface [22]. At nonzero Reynolds number, both the inertial and elastic mechanisms are operative in a viscoelastic liquid. The stability of film flows down an inclined plane has also been generalized to Newtonian two-layer flows [23–26], and here the liquid-liquid interface was shown to become unstable even at zero Reynolds number, owing to the interaction between the free surface and the liquid-liquid interface. This study has been extended to two-layer viscoelastic film flows as well [27]. The presence of insoluble surfactants at the free surface, in general, results in the stabilization of the free-surface instability, and thereby increases the critical Reynolds number for destabilization. Blyth and Pozrikidis [16] showed that the effect of an insoluble surfactant is stabilizing on the classical instability of Yih, but there arises a new "Marangoni" mode associated with the periodic variation of surfactant concentration, which, however, remains stable. Thus, they concluded that the surfactant has a stabilizing effect on the interfacial dynamics of film flows. Shkadov *et al.* [17] considered solubility of the surfactant molecules by accounting for adsorption and desorption from the free surface, and showed that *four* new modes appear in addition to the free-surface instability due to Marangoni-driven diffusion of surfactants, while the free-surface mode itself is stabilized by the Marangoni effect. Recently, Wei [18,19] studied the stability of viscoelastic film flow in the presence of surfactants and interfacial shear. Application of interfacial shear was found to destabilize the Marangoni mode and stabilize the elasticity induced instability depending on the strength and direction of the applied interfacial shear.

While the above-mentioned studies focused on the nature of the free-surface instability *per se* in various systems, there have also been some studies which explored the possibility of controlling the free-surface instability by different methods. Lin *et al.* [10] studied the effect of in-plane horizontal oscillations (in the direction parallel to the flow) in the inclined plate on the free-surface instability using Floquet theory. They showed that, by use of appropriate amplitudes and frequencies of the forced oscillations, it is possible to suppress the free-surface instability of the liquid film flow. A similar conclusion was reached by Jiang and Lin [12] on the effect of horizontal oscillations on two-layer liquid film flow. The strategy of imposing wall oscillations has also been extended to viscoelastic film flows down an inclined plane by Khomami and co-workers [13,14]. More recently, Demekhin *et al.* [15] explored the possibility of using heating of the inclined surface by a linearly increasing temperature distribution, and showed that, at small Prandtl numbers, the temperature gradient leads to stabilization of all the unstable modes.

These suggestions for instability suppression may be categorized as "active" methods (i.e., externally imposed oscillations or heating of the plate) toward suppressing the free-surface instability. In the present study we examine the feasibility of a "passive" method, where a deformable solid coating is proposed for suppressing the free-surface instability in viscoelastic film flows. The elastohydrodynamic coupling between fluid flow and solid deformation is well known to *induce* instabilities at the *liquid-solid* interface, leading to the formation of interfacial waves, as shown (by both theory and experiments) in Refs. [28–31]. There has also been some work [32] on the effect of deformability of the wall on the capillary instability of an annular liquid film coated inside a cylindrical elastic shell. Here, the base state is a stationary liquid film of uniform thickness, which is destabilized by curvature-induced capillary forces. The concomitant pressure variations in the liquid film induce a deformation in the shell as well, which in turn enhances the instability of the liquid film.

In this study, we examine the opposite possibility of instability *suppression* at the *free surface* of viscoelastic liquids by employing a deformable solid layer. Toward this end, it is important to realize that both the solid and the liquid layers can admit waves in isolation, and, when coupled together, it is crucial to ensure that no new additional instabilities are induced in the coupled liquid-solid system [33]. Previous studies on Newtonian film flow past a deformable solid have shown that while the long-wave free-surface instability was suppressed by the deformable solid layer, increasing the deformability of the solid further induced finite wavelength instabilities in the system. Further, for a range of shear modulus of the solid, it was shown that there are no instabilities at any wave number, thus making deformable solid coatings potential candidates for instability suppression. The numerical methodology used to arrive at this conclusion was based on a Newton-Raphson iteration of the characteristic equation (obtained by numerically integrating the governing differential equations) supplemented by asymptotic solutions at low wave number and zero Reynolds number. However, at finite wave number and inertia in the fluid, it is now well known that many new unstable modes proliferate, owing to the coupling between the free shear waves in the elastic solid and the liquid flow [34,35]. These "inertial" modes in the coupled liquid-solid system are not accessible to the Newton-Raphson iterative method without the presence of a good initial guess for the solution. Thus, while the previous predictions [20,21] are indicative of instability suppression, they are not conclusive, because it is necessary to determine the complete spectrum of eigenvalues in order to demonstrate instability suppression by the deformable solid layer. To address this limitation, in the present work, we undertake a spectral Chebyshev-Tau [36,37] numerical solution of the governing equations, which yields the complete spectrum of eigenvalues without requiring any initial guess.

It is also pertinent here to remark on the rheological constitutive relations used to describe the liquid and solid layers in this study. We use the Oldroyd-B–upper-convected Max-

well class of models [38,39] to describe the rheology of the liquid layer, as these models retain the essential qualitative physics necessary to capture the free-surface instability in polymeric liquids. The Oldroyd-B model attempts to describe the rheological behavior of polymer solutions, wherein a polymer molecule is coarse grained by a "dumbbell" consisting of two beads which act as the source of hydrodynamic resistance, connected by an infinitely extensible "spring" which mimics the entropic elasticity of a single polymer molecule. This model predicts a first-normal stress difference in simple shear flow, but also predicts a shear-rate-independent viscosity, unlike real polymeric liquids. For the solid layer, while many theoretical studies in the area have used the linear elastic model for describing the deformation in the solid, recently Gkanis and Kumar [30,40] pointed out that the linear elastic model is strictly valid only when the strain in the solid layer is small, and that appropriate modifications must be made at finite deformations in order to obey the principle of material-frame indifference [41,42]. In lieu of the linear elastic solid, they suggested the use of a neo-Hookean model, which is a frame-invariant generalization of the Hookean model for solids, and is applicable for finite and large deformations [43] typically encountered in soft solid materials such as elastomers. The neo-Hookean solid yields a first-normal stress difference in the base state, and the discontinuity of this normal stress in the base state at the liquid-solid interface was shown to give rise to a short-wave instability, which is absent in linear viscoelastic solids. In this study, therefore, we employ the neo-Hookean constitutive relation to determine the solid deformation. The remainder of this paper is organized as follows. Section II A presents the governing equations and boundary conditions, and Sec. II B describes the base-state velocity and stresses in both the liquid and solid layers. The linearized governing equations along with interface conditions are given in Sec. II C. A low-wave-number asymptotic analysis is carried out in Sec. III A, and the numerical methods used in this study are outlined in Sec. III B. The main results from our numerical solution are discussed in Sec. IV, and we end with the salient conclusions in Sec. V.

II. PROBLEM FORMULATION

The system consists of an incompressible viscoelastic liquid flowing past an incompressible and impermeable deformable solid. The solid is strongly bonded to a rigid inclined plane at $z^*=(1+H)R$ and makes an angle θ with the horizontal as shown in Fig. 1. The polymeric liquid is modeled using the Oldroyd-B model [38,39], and the stress in this model can be regarded as originating from two contributions: a viscoelastic contribution from the bead-spring units and a viscous contribution from the solvent; this model has three material constants: the shear-rate-independent viscosity μ, relaxation time τ_R, and a nondimensional ratio of solvent to polymeric contribution to the viscosity. In what follows, the density of the fluid is denoted by ρ and g is the gravitational acceleration; μ_s and μ_p are the viscosities of pure solvent and pure polymer, respectively; hence the total viscosity of the solution is given by $\mu=\mu_s+\mu_p$. The liquid layer is in contact with a passive gas and occupies a region $0\leq z^*\leq R$. The thickness of the solid layer is HR and its shear modulus is G. In what follows, we denote dimensional variables with an asterisk, and nondimensional variables without any superscript. It is convenient to nondimensionalize various physical quantities by using the following scales: lengths and displacements by R; velocities by $\rho g R^2 \sin\theta/2\mu \equiv V$, which is the free-surface velocity of the liquid layer; time by R/V; pressure and solid stresses by $\mu V/R$; polymeric stresses by $\mu_p V/R$; and solvent stresses by $\mu_s V/R$.

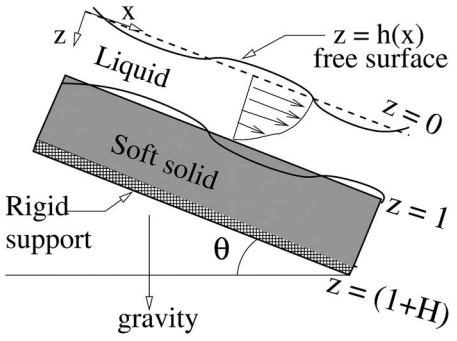

FIG. 1. Schematic diagram of the flow configuration and nondimensional coordinate system.

A. Governing equations

The nondimensional equations governing the dynamics of the liquid are the mass and momentum conservation equations:

$$\nabla \cdot \mathbf{v} = 0, \tag{1}$$

$$\mathrm{Re}\left(\frac{\partial \mathbf{v}}{\partial t} + \mathbf{v}\cdot\nabla\mathbf{v}\right) = \nabla\cdot\mathbf{T} + \frac{2}{\sin\theta}\hat{\mathbf{g}}. \tag{2}$$

Here, $\mathbf{v}$ represents the velocity field in the liquid, $\hat{\mathbf{g}}$ is the unit vector pointing in the direction of gravity, and $\mathrm{Re}=\rho V R/\mu$ is the Reynolds number. $\mathbf{T}=-p_f\mathbf{I}+\boldsymbol{\tau}$ is the total stress tensor in the fluid, which is the sum of an isotropic pressure $-p_f\mathbf{I}$ and the extra-stress tensor $\boldsymbol{\tau}=\beta\boldsymbol{\tau}^s+(1-\beta)\boldsymbol{\tau}^p$. Here $\beta=\mu_s/\mu$ is the ratio of the solvent viscosity to the total viscosity. The solvent contribution to the extra-stress tensor $\boldsymbol{\tau}$ is represented by $\boldsymbol{\tau}^s=[\nabla\mathbf{v}+(\nabla\mathbf{v})^T]$, while $\boldsymbol{\tau}^p$ is the polymeric contribution to the extra-stress tensor, which is given by the Oldroyd-B constitutive relation [7,39]

$$W\left(\frac{\partial\boldsymbol{\tau}^p}{\partial t} + \mathbf{v}\cdot\nabla\boldsymbol{\tau}^p - (\nabla\mathbf{v})^T\cdot\boldsymbol{\tau}^p - \boldsymbol{\tau}^p\cdot\nabla\mathbf{v}\right) + \boldsymbol{\tau}^p = \nabla\mathbf{v} + (\nabla\mathbf{v})^T, \tag{3}$$

where $W\equiv\tau_R V/R$ is the nondimensional Weissenberg number characterizing the relaxation time of the viscoelastic fluid. If we set the ratio of solvent to total viscosity β to zero, then we obtain the upper-convected Maxwell (UCM) model which attempts to describe the rheology of polymer melts without any solvent. The deformable solid wall is modeled as an incompressible solid and is described by the neo-Hookean model [30,40,42,43]. The deformation field satisfies the mass and momentum conservation equations [42]

$$\det(\mathbf{F}) = 1, \tag{4}$$

$$\mathrm{Re}\left(\frac{\partial^2 \boldsymbol{w}}{\partial t^2}\right)_{\boldsymbol{X}} = \boldsymbol{\nabla}_{\boldsymbol{X}} \cdot \mathbf{P} + \frac{2}{\sin\theta}\hat{\mathbf{g}}. \tag{5}$$

The above two equations are similar to the ones used by Gkanis and Kumar [30] except that inertia is included here and a different nondimensionalization scheme is used. The deformation gradient tensor is defined as $\mathbf{F}=\boldsymbol{\nabla}_{\boldsymbol{X}}\boldsymbol{w}$, where $\boldsymbol{w}(\mathbf{X})$ represents the position vector of a particle in the current configuration of the neo-Hookean solid. The capital letter $\mathbf{X}=(X,Y,Z)$ denotes the spatial coordinates in the reference (i.e., unstressed) configuration and hence the subscript $\mathbf{X}$ in (5) indicates the gradient with respect to the reference coordinates. The Lagrangian displacement vector of material points is given by $\mathbf{u}(\mathbf{X})=\boldsymbol{w}(\mathbf{X})-\mathbf{X}$. For the liquid, the (x,y,z) coordinate system is used, and this coordinate system coincides with the reference coordinate system (X,Y,Z) for the neo-Hookean solid.

The first Piola Kirchhoff stress tensor $\mathbf{P}$ is related to the Cauchy stress tensor by $\mathbf{P}=\mathbf{F}^{-1}\cdot\boldsymbol{\sigma}$, where the Cauchy stress tensor for a neo-Hookean solid is given by [42,43]

$$\boldsymbol{\sigma} = -\hat{p}_s\mathbf{I} + \frac{1}{\Gamma}(\mathbf{F}\cdot\mathbf{F}^T), \tag{6}$$

where $\hat{p}_s$ is the pressurelike function related to actual pressure in a neo-Hookean solid as $\hat{p}_s=p_s+1/\Gamma$. Here, $\Gamma=\mu V/GR=\rho gR\sin\theta/2G$ is the ratio of gravitational forces in the liquid to elastic forces in the solid, and is a measure of the deformability in the solid layer; here G is the shear modulus of the solid.

In this study, the densities of liquid and solid are assumed to be equal without loss of generality. If the densities are different, then the ratio of solid to liquid densities ρ_s/ρ_l will appear in the left side of the momentum Eq. (5). The low-wave-number ($k\ll 1$) asymptotic analysis carried out subsequently (Sec. III A) shows that, to leading order in wave number, inertial stresses in the solid are $O(k^2)$ smaller than the elastic stresses, and the inertial stresses of the solid layer do not appear in the low-wave-number limit. Therefore the low-wave-number asymptotic results are expected to be valid for any value of the ratio ρ_s/ρ_l. At finite wave numbers, the inertial stresses could become comparable to the elastic stresses in the solid layer, and in such cases, there will be some quantitative difference in the results when the ratio $\rho_s/\rho_l\neq 1$. However, the qualitative predictions of the present study are expected to remain unaltered due to the change in density ratio.

The conditions at the free surface are the kinematic condition for evolution of the free surface and tangential and normal stress balances. The tangential stress at the free surface is zero and the normal stress in the liquid is balanced by the hydrostatic pressure in the gas adjacent to it:

$$\partial_t h + v_x\partial_x h = v_z, \tag{7}$$

$$\mathbf{n}\cdot\mathbf{T}\cdot\mathbf{t} = 0, \tag{8}$$

$$\mathbf{n}\cdot\mathbf{T}\cdot\mathbf{n} = \Sigma_f(\boldsymbol{\nabla}\cdot\mathbf{n}), \tag{9}$$

where h is the free-surface position, $\mathbf{n}$ and $\mathbf{t}$ are the normal and tangential unit vectors to the free surface, respectively, and $\Sigma_f=\gamma_f/\mu V$ is the nondimensional surface tension parameter at the free surface, with γ_f being the dimensional surface tension at the free surface. At a liquid-solid interface the velocities and stresses in liquid and solid layers are continuous. The condition of velocity continuity is given as

$$\mathbf{v} = \frac{\partial \boldsymbol{w}}{\partial t}. \tag{10}$$

The normal and tangential stress balance is given as

$$\mathbf{n}\cdot\mathbf{T}\cdot\mathbf{t} = \mathbf{n}\cdot\boldsymbol{\sigma}\cdot\mathbf{t}, \tag{11}$$

$$\mathbf{n}\cdot\boldsymbol{\sigma}\cdot\mathbf{n} - \mathbf{n}\cdot\mathbf{T}\cdot\mathbf{n} = \Sigma_i(\boldsymbol{\nabla}\cdot\mathbf{n}). \tag{12}$$

Here, $\mathbf{n}$ and $\mathbf{t}$ are the normal and tangential unit vectors for the liquid-solid interface. $\Sigma_i=\gamma_i/\mu V$ is the nondimensional surface tension parameter, with γ_i being the dimensional liquid-solid interface tension. At the bottom rigid surface ($z=1+H$) the zero-displacement condition holds for the solid layer: $\boldsymbol{w}(\mathbf{X})=\mathbf{X}$.

B. Base state

The laminar base state of the present system consists of unidirectional flow of liquid in the x direction due to gravity. The solid layer is at rest in this steady state with a nonzero displacement in the x direction due to liquid shear stress at the interface. Both gas-liquid and liquid-solid interfaces remain flat in the base state. The nondimensional velocity profile, pressure distribution, and polymeric stresses in the liquid layer are given as

$$\bar{v}_x = 1 - z^2, \tag{13}$$

$$\bar{v}_z = 0, \tag{14}$$

$$\bar{p} = 2z\cot\theta, \tag{15}$$

$$\bar{\tau}^p_{zz} = 0, \tag{16}$$

$$\bar{\tau}^p_{xz} = -2z, \tag{17}$$

$$\bar{\tau}^p_{xx} = 8Wz^2. \tag{18}$$

The base-state quantities are represented with an overbar in this paper. The displacement and pressure field for a neo-Hookean solid are given by

$$\bar{w}_X = X + \Gamma[(1+H^2) - Z^2], \tag{19}$$

$$\bar{w}_Z = Z, \tag{20}$$

$$\bar{\hat{p}}_s = \frac{1}{\Gamma} + 2Z\cot\theta. \tag{21}$$

As pointed out by Gkanis and Kumar [30], the displacement field for both linear and neo-Hookean models remains the

same; however, there exists a nonzero first-normal stress difference for a neo-Hookean solid. This first-normal stress difference is equal to $(\sigma_{xx}-\sigma_{zz})=4\Gamma^2$ and it may cause a high-wave-number instability in the liquid-solid interface [30,40].

C. Linearized governing equations

A temporal linear stability analysis is performed in order to determine the stability of the coupled solid-liquid system. All the dynamical quantities (velocities, displacement, pressure, etc.) are perturbed about the base state and are substituted in the governing equations. The resulting equations are then linearized about the base state to obtain a set of equations in terms of the perturbation quantities. The perturbations are expanded in the form of Fourier modes,

$$f' = \tilde{f}(z)\exp[ik(x-ct)], \tag{22}$$

where f' is the perturbation to any physical variable, k is the wave number of perturbations, c is the complex wave speed, and $\tilde{f}(z)$ is the complex amplitude function of the disturbance. For the neo-Hookean model, x and z are replaced by X and Z, respectively. The imaginary part of the complex wave speed determines the stability of the system, and the system is unstable (stable) if $c_i>0$ (<0). When the above form of perturbations is substituted in the linearized perturbation equations and boundary conditions, one obtains a set of equations in terms of amplitude functions and wave speed c that govern the stability of the system.

Thus, the linearized governing equations for the liquid layer are (with $d_z \equiv d/dz$)

$$d_z\tilde{v}_z + ik\tilde{v}_x = 0, \tag{23}$$

$$\mathrm{Re}[ik(\bar{v}_x-c)\tilde{v}_x + (d_z\bar{v}_x)\tilde{v}_z] = -ik\tilde{p} + \beta(d_z^2\tilde{v}_x - k^2\tilde{v}_x) + (1-\beta)(ik\tilde{\tau}^p_{xx} + d_z\tilde{\tau}^p_{xz}), \tag{24}$$

$$\mathrm{Re}[ik(\bar{v}_x-c)\tilde{v}_z] = -d_z\tilde{p} + \beta(d_z^2\tilde{v}_z - k^2\tilde{v}_z) + (1-\beta)(ik\tilde{\tau}^p_{xz} + d_z\tilde{\tau}^p_{zz}). \tag{25}$$

The above equations can be combined to give a single fourth-order, Orr-Sommerfeld-like equation for $\tilde{v}_z$:

$$ik\,\mathrm{Re}[(\bar{v}_x-c)(d_z^2-k^2) - d_z^2\bar{v}_x]\tilde{v}_z = \beta(d_z^2-k^2)^2\tilde{v}_z + (1-\beta)\times[k^2d_z(\tilde{\tau}^p_{xx}-\tilde{\tau}^p_{zz}) - ik(d_z^2+k^2)\tilde{\tau}^p_{xz}], \tag{26}$$

where $\tilde{\tau}^p_{zz}$, $\tilde{\tau}^p_{xz}$, and $\tilde{\tau}^p_{xx}$ are obtained from the linearized constitutive Eq. (3):

$$[1+Wik(\bar{v}_x-c)]\tilde{\tau}^p_{zz} = 2(ikW\tilde{\tau}^p_{xz}\tilde{v}_z + d_z\tilde{v}_z), \tag{27}$$

$$[1+Wik(\bar{v}_x-c)]\tilde{\tau}^p_{xz} = Wd_z\bar{v}_x\tilde{\tau}^p_{zz} - [Wd_z\tilde{\tau}^p_{xz} - ik(1+W\tilde{\tau}^p_{xx})]\tilde{v}_z + d_z\tilde{v}_x, \tag{28}$$

$$[1+Wik(\bar{v}_x-c)]\tilde{\tau}^p_{xx} = 2Wd_z\bar{v}_x\tilde{\tau}^p_{xz} - Wd_z\tilde{\tau}^p_{xx}\tilde{v}_z + [2ik(1+W\tilde{\tau}^p_{xx})]\tilde{v}_x + 2W\tilde{\tau}^p_{xz}d_z\tilde{v}_x. \tag{29}$$

The governing linearized equations for the neo-Hookean solid model are

$$\frac{d\tilde{w}_Z}{dZ} + ik\tilde{w}_X + (2\Gamma Z)ik\tilde{w}_Z = 0, \tag{30}$$

$$-ik\tilde{p}_s + (2\cot\theta)ik\tilde{w}_Z + \frac{1}{\Gamma}\left(-k^2\tilde{w}_X + \frac{d^2\tilde{w}_X}{dZ^2}\right) = -k^2c^2\mathrm{Re}\,\tilde{w}_X, \tag{31}$$

$$-(2\Gamma X_2)ik\tilde{p}_s - (2\cot\theta)ik\tilde{w}_X - \frac{d\tilde{p}_s}{dZ} + \frac{1}{\Gamma}\left(-k^2\tilde{w}_Z + \frac{d^2\tilde{w}_Z}{dZ^2}\right) = -k^2c^2\mathrm{Re}\,\tilde{w}_Z. \tag{32}$$

These equations can be condensed in a single fourth-order, Orr-Sommerfeld-like equation for $\tilde{w}_Z$. In both the above two sets of governing equations, the first equation represents the continuity or mass conservation equation, and the next two equations represent the x and z momentum balance, respectively. The interfacial conditions at the free surface and liquid-solid interface are linearized by Taylor-expanding the conditions about their respective mean interface positions [20,40]. Hence, the linearized kinematic and boundary conditions at the unperturbed free surface $(z=0)$ are

$$ik(\bar{v}_x-c)\tilde{h} = \tilde{v}_z, \tag{33}$$

$$\beta\left[-2\tilde{h} + \left(\frac{d\tilde{v}_x}{dz} + ik\tilde{v}_z\right)\right] + (1-\beta)\left(\tilde{\tau}^p_{xz} + \frac{d\bar{\tau}^p_{xx}}{dz}\tilde{h}\right) = 0, \tag{34}$$

$$-\tilde{p} - (2\cot\theta)\tilde{h} - k^2\Sigma_f\tilde{h} + 2\beta\frac{d\tilde{v}_z}{dz} + (1-\beta)\tilde{\tau}^p_{zz} = 0. \tag{35}$$

Similarly, the linearized boundary conditions at the liquid-solid interface $(z=1)$ are

$$\tilde{v}_z = -ikc\tilde{w}_Z, \tag{36}$$

$$\tilde{v}_x + \tilde{w}_Z(d_z\bar{v}_x)_{z=1} = -ikc\tilde{w}_X, \tag{37}$$

$$(-4\Gamma^2)ik\tilde{w}_Z - (2\Gamma)\frac{d\tilde{w}_Z}{dZ} + ik\tilde{w}_Z + \frac{d\tilde{w}_X}{dZ} = (1-\beta)(\Gamma\tilde{\tau}^p_{xz} + 8ikW\Gamma\tilde{w}_Z) + \beta\Gamma\left(\frac{d\tilde{v}_x}{dz} + ik\tilde{v}_z\right), \tag{38}$$

$$-\tilde{p}+2\beta\frac{d\tilde{v}_Z}{dz}+(1-\beta)\tilde{\tau}^p_{ZZ}+\tilde{p}_s-\frac{2}{\Gamma}\frac{d\tilde{w}_Z}{dZ}+k^2\Sigma_i\tilde{w}_Z=0. \tag{39}$$

In the boundary conditions at the liquid-solid interface, the first two equations are the conditions for continuity of velocities and the next two represent the balance of tangential and normal forces, respectively. Finally, the boundary conditions at the rigid surface ($z=1+H$) are $\tilde{\boldsymbol{w}}=0$. This completes the description of equations that govern the stability of the system, and the resulting set of equations can be solved for complex wave speed c as a function of the parameters Re, W, β, k, θ, Γ, H, Σ_f, and Σ_i.

III. SOLUTION METHODOLOGY

The free-surface interfacial mode is traditionally analyzed using a low-wave-number asymptotic analysis, following the classical work of Yih [2]. For the case of viscoelastic flow down an inclined plane, a similar analysis was carried out by Gupta [4,5] and Lai [6], and subsequently by Shaqfeh *et al.* [7]. In this section, we first generalize these long-wave analyses for viscoelastic liquids to include the presence of a deformable solid layer, which is the focus of the present work. In order to extend these low-k results to finite wave numbers, we have employed two different numerical methods: first, a Chebyshev-Tau spectral method [36,37], which gives us the complete spectrum of eigenvalues for c with specified values of remaining parameters, and second, an orthonormal numerical shooting procedure [44] combined with a Newton-Raphson method to solve the characteristic equation for the eigenvalue c.

A. Low-wave-number analysis

The low-wave-number analysis of Yih [2] is extended here to the case of viscoelastic liquid flow past a neo-Hookean solid. The method is similar to that used by Shankar and Sahu [20] for Newtonian liquid flow past a linear elastic solid, and we provide only the key steps involved in the analysis, and the central result from the analysis. For low wave numbers ($k \ll 1$), the complex wave speed corresponding to the free-surface mode is expanded in an asymptotic series in k:

$$c=c^{(0)}+kc^{(1)}+\cdots. \tag{40}$$

If we set $\tilde{v}_x \sim O(1)$, then the continuity Eq. (23) implies $\tilde{v}_z \sim O(k)$ and the x momentum Eq. (24) implies $\tilde{p} \sim O(k^{-1})$. Therefore, the velocities and pressure in the fluid are expanded as

$$\tilde{v}_x=\tilde{v}_x^{(0)}+k\tilde{v}_x^{(1)}+\cdots, \quad \tilde{v}_z=k\tilde{v}_z^{(0)}+k^2\tilde{v}_z^{(1)}+\cdots, \tag{41}$$

$$\tilde{p}=k^{-1}\tilde{p}^{(0)}+\tilde{p}^{(1)}+\cdots. \tag{42}$$

Similarly, the displacement field and the pressure in the solid layer are expanded as

$$\tilde{w}_X=\tilde{w}_X^{(0)}+k\tilde{w}_X^{(1)}+\cdots, \quad \tilde{w}_Z=k\tilde{w}_Z^{(0)}+k^2\tilde{w}_Z^{(1)}+\cdots, \tag{43}$$

$$\tilde{p}_s=k^{-1}\tilde{p}_s^{(0)}+\tilde{p}_s^{(1)}+\cdots. \tag{44}$$

The Fourier coefficient of the free-surface height fluctuation $\tilde{h} \sim O(1)$ as indicated by Eq. (33). We therefore expand $\tilde{h}=\tilde{h}^{(0)}+k\tilde{h}^{(1)}+\cdots$.

The following differential equations determine the leading-order and first correction to the fluid velocity field:

$$\beta d_z^4\tilde{v}_z^{(0)}-i(1-\beta)d_z^2\tilde{\tau}_{xz}^{p(0)}=0, \tag{45}$$

$$\beta d_z^4\tilde{v}_z^{(1)}-i(1-\beta)d_z^2\tilde{\tau}_{xz}^{p(1)} = i\,\mathrm{Re}[(\bar{v}_x-c)d_z^2-d_z^2\bar{v}_x]\tilde{v}_z^{(0)}+(1-\beta)d_z(\tilde{\tau}_{zz}^{p(0)}-\tilde{\tau}_{xx}^{p(0)}). \tag{46}$$

It turns out that the leading-order displacement field is sufficient in the present low-k analysis, and it is governed by the following differential equation:

$$d_{X_3}^4\tilde{w}_Z^{(0)}=0. \tag{47}$$

The boundary and interface conditions for the leading-order problem are obtained by substituting the asymptotic expansions in Eqs. (33)–(39). This results in the following conditions at $z=0$:

$$-2(1-\beta)\tilde{h}^{(0)}+(1-\beta)\tilde{\tau}_{xz}^{p(0)}+\beta k\frac{d\tilde{v}_x^{(0)}}{dz}-2\beta\tilde{h}^{(0)}=0, \tag{48}$$

$$-\tilde{p}^{(0)}=0. \tag{49}$$

The leading-order conditions at the fluid-solid interface $z=1$ are given by

$$\tilde{v}_z^{(0)}=0, \tag{50}$$

$$\tilde{v}_x^{(0)}=0, \tag{51}$$

$$\beta\Gamma\frac{d\tilde{v}_x^{(0)}}{dz}+(1-\beta)\Gamma\tilde{\tau}_{xz}^{p(0)}=\frac{d\tilde{w}_X^{(0)}}{dZ}, \tag{52}$$

$$\tilde{p}^{(0)}=\tilde{p}_s^{(0)}. \tag{53}$$

The boundary conditions at $z=1+H$ are simply

$$\tilde{w}_Z^{(0)}=0, \quad \tilde{w}_X^{(0)}=0. \tag{54}$$

In the low-k limit, the interface conditions [Eqs. (36) and (37)] indicate that the velocities $\tilde{v}_z^{(0)}$ and $\tilde{v}_x^{(0)}$ satisfy the no-slip conditions at $z=1$ to leading order in the analysis, as in a rigid boundary [Eqs. (50) and (51)]. Thus, the solid-layer deformability does not influence the leading-order fluid velocity field, and so the leading-order wave speed in the present problem must be identical to that of Gupta [4,5] and Lai's [6] analysis. However, the leading-order velocity field in the liquid layer exerts a shear stress on the solid layer via the tangential stress condition [Eq. (52)], and this causes a deformation in the solid layer at leading order. This deformation field in the solid layer affects the first correction to the wave speed at $O(k)$ in the analysis, in a manner similar to

that found for Newtonian liquids in Ref. [20]. In the interests of brevity, we provide only the final result from our asymptotic analysis:

$$c^{(0)} = 2, \tag{55}$$

$$c^{(1)} = \frac{2i}{15}\{[4\mathrm{Re} + 10W(1-\beta) - 5\cot\theta] - 30\Gamma H\}. \tag{56}$$

To leading order, we obtain neutrally stable waves, and the first correction $c^{(1)}$ dictates the stability or instability of the system depending on the parameters Re, W, θ, Γ, β, and H. In the above result for $c^{(1)}$, the terms inside the square brackets are identical to those found in Refs. [5] and [6] for viscoelastic film flows down a rigid incline. The term involving the product ΓH denotes the effect of the solid layer deformability on the free-surface mode. There are several interesting features in the above result: First, the leading-order wave speed is identical to that found in Yih's [2] analysis (except for the different scheme of nondimensionalization used here) for Newtonian liquids, and Lai's [6] result for viscoelastic liquids. Second, in the limit of a rigid inclined plane obtained by setting Γ or $H=0$, the above result reduces to that of Gupta and Rai [4,5] and Lai [6]. Third, the contribution due to the soft solid layer is stabilizing, and is identical to the earlier result of Ref. [20] for Newtonian fluids past a linear elastic solid. Thus, our analysis reveals that the rheological nature of the liquid (Newtonian vs viscoelastic) and the solid (linear elastic vs neo-Hookean) has no consequence on the effect of the deformable solid layer in the low-wave-number limit. This can further be understood by noting that the leading-order velocity fields and wave speed in viscoelastic liquids are identical to those in the Newtonian case, and therefore the deformation field set up in the solid due to the liquid stresses also remains unchanged when one proceeds from Newtonian to viscoelastic liquids. This deformation field in the solid is responsible for the stabilizing contribution proportional to ΓH in the first correction $c^{(1)}$, and hence this remains identical to the Newtonian case. Further, when one compares the linear elastic model used in Ref. [20] to the neo-Hookean model in the present study, again one can verify that the additional contributions to the linearized stability equations in the neo-Hookean model remain subdominant for $k \ll 1$, and both the models reduce to identical sets of equations in this limit. For these reasons, the stabilizing nature of the solid layer remains invariant to changes in the constitutive nature of the liquid and solid layers in the low-k limit.

In Ref. [20], it was shown that the first correction to the wave speed, which determines the stability of the free-surface mode, is directly related to the first correction to the shear stress in the liquid at the free surface. The destabilizing terms due to fluid elasticity and inertia (proportional, respectively, to W and Re) appear only in the first correction to the fluid velocity field. In addition to these destabilizing contributions, and in contrast to a rigid surface, the deformation in the soft solid layer creates a perturbation flow via the shear-stress continuity condition, which also appears at $O(k)$. Physically, the perturbation flow at $O(k)$ due to the solid deformation opposes the flow due to viscoelastic and inertial effects, thus resulting in stabilization of the free-surface instability. In particular, the free-surface instability is completely suppressed in the low-wave-number limit if

$$30\Gamma H > [4\mathrm{Re} + 10W(1-\beta) - 5\cot\theta]. \tag{57}$$

The above equation can be recast to yield a condition for instability in terms of Re: The flow is unstable for $\mathrm{Re} > \mathrm{Re}_c$, where $\mathrm{Re}_c = (5/4)\cot\theta - (5/2)W(1-\beta) + (15/2)\Gamma H$. This criterion also demonstrates the role of the different effects: when W increases, Re_c decreases, implying the destabilizing influence of fluid viscoelasticity. On the other hand, when Γ increases, Re_c increases, indicating that wall deformability is stabilizing.

However, this result is valid only for perturbations with wavelengths large compared to the film thickness. In order to realize the predicted stabilization in an experiment, it is necessary to extend these results to perturbations with arbitrary wavelengths. This is done using two different numerical methods, as described below.

B. Numerical methods

In the previous studies [20,40], a numerical Runge-Kutta integrator was employed to determine the linearly independent solutions [44] in the solid and liquid layers, and the interfacial conditions were used to set up a characteristic matrix, whose determinant was set to zero in order to determine the complex wave speed c. A Newton-Raphson iterative technique was employed to solve the characteristic equation, which requires a good initial guess to converge to the desired eigenvalue. In Ref. [20], the low-k asymptotic analytical result for the free-surface mode was used as a starting guess for the above numerical method, in order to continue the low-k result to finite wave numbers. An important feature of systems involving flow past deformable solid media is that the fluid-solid interaction itself could give rise to a host of new instabilities [28,34,35] at the fluid-solid interface. In the previous study [20], a zero-Re analytical solution was used to predict the "liquid-solid" mode, and this was further used as an initial guess for the above numerical procedure. However, at finite Re and Γ, there is no guarantee that the only unstable eigenvalues are those corresponding to the free-surface mode and the liquid-solid mode continued from the Re=0 analysis. Indeed, previous studies [34,35,45] have shown that, at finite inertia, the shear waves in an elastic solid are modified by the flow, and these become unstable at finite Re. Thus, any claim of instability suppression in flow past a deformable solid must be supported by a numerical methodology that gives rise to all the eigenvalues in the problem, and not just the ones amenable to asymptotic analysis. To address this issue, we have implemented the Chebyshev-Tau spectral method, pioneered by Orszag [36,37,46], for the present problem. The spectral method has the twin advantages that it does not need any initial guess, and it provides the complete eigenspectrum for the given problem. In the Chebyshev-Tau method, the unknown variables (e.g., velocity field in the fluid and displacement field in the solid) are expanded in a truncated series of N Cheby-

shev polynomials. These expansions are substituted in the linearized governing equations, and the resulting equations are made orthonormal to the first $N-8$ Chebyshev polynomials to yield $N-8$ equations for the unknown coefficients. The remaining eight equations are obtained from the boundary and interface conditions. This yields a matrix eigenvalue problem for c, which is solved using the "polyeig" eigenvalue solver in MATLAB. To filter out the spurious eigenmodes that may arise, the truncation level N is increased until the genuine modes are accurately identified. In addition, to check the veracity of the eigenmodes, we provide these as an initial guess to the orthonormal shooting procedure discussed above, and it is ensured that the eigenvalue obtained from the spectral code is indeed genuine.

Our spectral code was benchmarked with the results for several limiting cases available in the existing literature. First, we reproduced the neutral stability results of Shaqfeh *et al.* [7] for the problem of viscoelastic film flow down a rigid incline. Although Shaqfeh *et al.* carry out a spatial stability analysis (as opposed to the temporal analysis here), for neutrally stable modes, both the analyses reduce to the same results [44]. Second, we reproduced the earlier numerical results for Newtonian liquid flow down a deformable solid layer [21] by setting either $W=0$ or $\beta=1$. Third, we reproduced the low-k analytical results for the present problem in Sec. III A using our spectral code for small k. In all these cases, good agreement was found between our results and reported results. Apart from these validation tests for the spectral code, we have verified that the spectral results are captured by the orthonormal shooting procedure as well.

IV. RESULTS FROM NUMERICAL SOLUTION

In this section, we present results from the above numerical methods. The key objectives of the numerical solution are the following: First, to extend our low-k analytical result for instability suppression to finite and arbitrary values of wave number; second, to unambiguously determine the unstable modes caused by the deformability of the solid layer, and, consequently, to arrive at predictions for parameter values wherein there are no instabilities in the composite solid-liquid system. This would involve construction of "neutral stability curves" for various unstable modes that demarcate stable and unstable regions in an appropriate parameter space.

A. Estimation of parameters

At the outset, we estimate the orders of magnitude of various nondimensional groups involved in the problem, which will guide us in choosing these parameters for the subsequent numerical results. The key parameter denoting the deformability of the solid layer is $\Gamma \equiv \rho g R \sin\theta/2G \sim \rho g R/G$. Upon using $\rho \sim 10^3$ kg/m^3, $g \sim 10$ m/s^2, and $G \sim 10^3$ Pa for very soft solids, we obtain $\Gamma \sim 10R$, and thus $\Gamma \sim 0.1$ for films with $R \sim 10^{-2}$ m. The Reynolds number $\mathrm{Re} \sim \rho^2 g R^3/\mu^2$ is estimated here for polymer melts and polymer solutions separately. For polymer melts, following the Appendix of Shaqfeh *et al.* [7], $\mu \sim 10^2 - 10^3$ Pa s, relaxation time $\tau_R \sim 10-100$ s, and so $\mathrm{Re} \sim 10^{-3} - 10^{-5}$, which is extremely small. Therefore, for polymer melts, it is appropriate to set $\mathrm{Re}=0$ in the following discussion. The Weissenberg number, which is a nondimensional relaxation time for the polymer, is estimated as $W \sim \tau_R \rho g R/\mu \sim 0.1-1$. For polymer solutions, again following Ref. [7], $\mu \sim 0.1-1$ Pa s, $\tau_R \sim 10^{-2}$ s, and thus we estimate $\mathrm{Re} \sim 10^{-2}-1$, $W \sim 1-10$. For the Oldroyd-B fluid, we set the ratio of solvent to total viscosity $\beta=0.5$ in the following discussion. The surface tension parameter at both the interfaces is estimated as $\Sigma \sim 0.1-1$, for dimensional interfacial tension $\gamma \sim 10^{-2}$ N/m. Other parameters include the nondimensional solid to fluid thickness ratio H, which is varied from 0.5 to 5, and angle of inclination θ, which is chosen to be 90° or 50°.

B. Mode structure and mode mixing

It is first useful to anticipate the types of modes present in the composite system that can potentially become unstable at different parametric regimes. The mode that is of primary concern here, of course, is the free-surface mode, which becomes unstable in a rigid incline, which can be recovered from the present problem by setting $\Gamma=0$. As Γ is increased, the solid layer becomes more deformable, and the free-surface mode is stabilized at low k as predicted by the asymptotic analysis in Sec. III A. When Γ is such that it satisfies Eq. (57), this low-k instability would be completely suppressed. Whether this predicted stabilization holds for finite k, and whether the solid deformability can destabilize this free-surface mode at finite k, will be explored below. In addition to this free-surface mode, there is another interfacial mode corresponding to the liquid-solid interface, which can become unstable at finite wave numbers when the parameter Γ becomes sufficiently large [28], even when $\mathrm{Re}=0$. For a neo-Hookean solid, this liquid-solid mode also has a high-wave-number branch [30,40], which is caused by the jump in first-normal stress at the solid-liquid interface. At $\mathrm{Re}=0$, in addition, there exist other stable modes in the composite liquid-solid system, which can be upstream traveling waves, whose stability is unaffected by wall deformability. At finite Re, inertial effects in the fluid and the solid become important, and a host of new modes corresponding to the coupled fluid-solid system could also become unstable when Γ is sufficiently large [34,35]. For polymer melts, since the Reynolds number is estimated to be very low, we therefore anticipate the possibility of only two modes corresponding to the free surface and liquid-solid interfaces.

Using our spectral method, we computed the spectrum at several values of Γ, and obtained the variation of c_i and c_r with the wave number k. The objective of this exercise is to determine whether the predicted stabilization of the free-surface mode holds for all wave numbers, and to determine whether or not there are other unstable modes due to the liquid-solid coupling. It must be noted here that the linearized governing equations for stability of the UCM fluid exhibit, in addition to the interfacial mode, a continuum of eigenvalues that arise when we set the coefficient multiplying the stress components in the linearized constitutive relations [Eqs. (27)–(29)] to zero. This yields the so-called con-

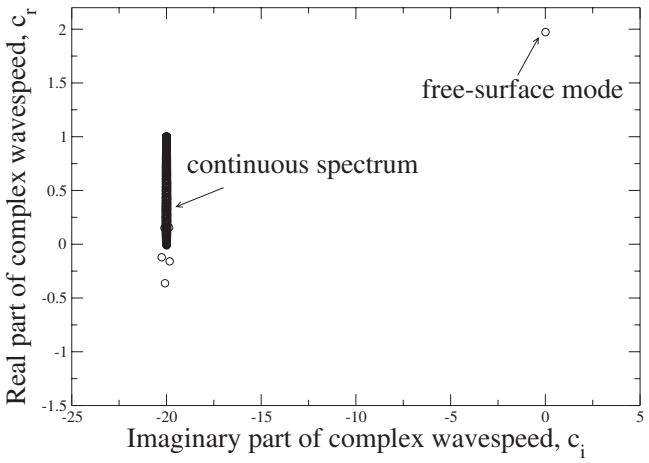

FIG. 2. Eigenvalue spectrum in the c_r-c_i plane for the UCM fluid showing the continuous spectrum and the unstable free-surface mode. Data for $\Gamma=0.001$, $k=0.1$, Re=0, $W=0.5$, $\beta=0$, $\theta=50°$, $H=1$, $\Sigma_f=2$, $\Sigma_i=1$.

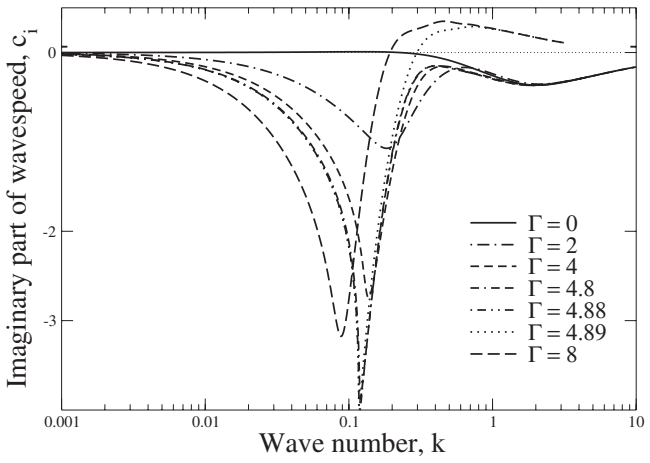

FIG. 4. Stabilization of mode 1 by the deformable solid layer at all wave numbers and the illustration of mode mixing: c_i vs k for $\beta=50°$, Re=0, $\beta=0$, $W=0.5$, $H=1$, $\Sigma_f=2$, $\Sigma_i=1$, and different values of Γ.

tinuous spectrum for viscoelastic liquids [47], which have $c_i=-1/(kW)$, and with c_r that can take values continuously between 0 and 1 (the maximum base-flow velocity; see Fig. 2). The continuous spectrum obtained from the spectral solution appears as a "balloon" (see Fig. 3) in the c_r-c_i plane, as has been noted in earlier studies [47]. Since the nature of the continuous spectrum is unaffected by the boundary conditions at the liquid-solid interface, the deformability of the solid has no effect on the continuous spectrum. In our spectral solution, we always observe this stable continuous spectrum of eigenvalues, and we find that the free-surface mode is well separated from this continuous spectrum as shown in Fig. 2. Therefore we eschew any discussion of the continuous spectrum and restrict our attention only on the free-surface mode hereafter. The free-surface mode was predicted to be stabilized in the low-k limit by the solid deformability. In Figs. 4 and 5, we show how this mode behaves as Γ is increased. For reasons that will become clear shortly, we shall also refer to this mode as mode 1. Figure 4 shows that, as Γ is increased from the rigid value ($\Gamma=0$), we find that the free-surface instability present in a rigid incline is completely suppressed at all wave numbers for $\Gamma=2$ and 4. One important feature of the free-surface mode in flow past a deformable solid is that, in the limits of both low ($k\ll 1$) and high ($k\gg 1$) wave numbers, we expect the c_r and c_i values for this mode (in the presence of solid deformability) to reduce to the result obtained for rigid surfaces. This is because, as $k\to 0$, our asymptotic analysis in Sec. III A shows that c_r is identical to that obtained in the rigid solid limit, and c_i is $O(k)$. For $k\gg 1$, which corresponds to very short wavelength perturbations, the perturbation velocity field corresponding to the free-surface mode will be localized near the free surface; hence one would expect the solid deformability to have no effect at $k\ll 1$ and $k\gg 1$. For Γ less than 4.89, this is indeed borne out in Figs. 4 and 5, respectively, for c_i and c_r

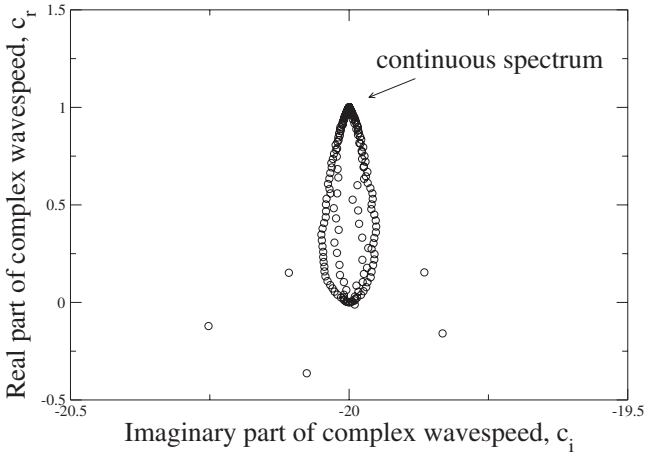

FIG. 3. Expanded view of the continuous spectrum in the c_r-c_i plane for the UCM fluid: Data same as in Fig. 2 ($\Gamma=0.001$, $k=0.1$, Re=0, $W=0.5$, $\beta=0$, $\theta=50°$, $H=1$, $\Sigma_f=2$, $\Sigma_i=1$).

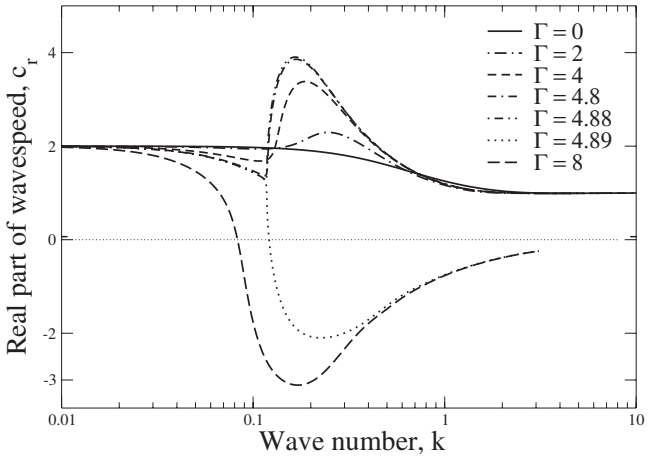

FIG. 5. Behavior of mode 1 for increasing values of solid deformability parameter Γ illustrating mode mixing: c_r vs k for $\beta=50°$, Re=0, $\beta=0$, $W=0.5$, $H=1$, $\Sigma_f=2$, $\Sigma_i=1$ (parameters same as in Fig. 4).

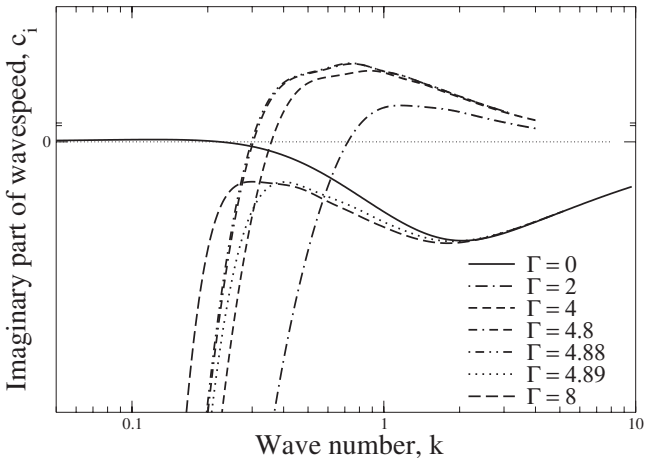

FIG. 6. Behavior of mode 2 plotted in terms of c_i vs k for increasing values of the solid deformability parameter: Mode mixing illustrated for $\beta=50°$, Re=0, $\beta=0$, $W=0.5$, $H=1$, $\Sigma_f=2$, $\Sigma_i=1$, and different values of Γ (parameters same as in Fig. 4).

vs k: the c_r and c_i curves for nonzero Γ (deformable solid) approach the behavior corresponding to the rigid surface limit ($\Gamma=0$) at low and high k. However, for $\Gamma\sim4.89$ and higher, we find that the c_i and c_r curves for mode 1 (continued from the low-k analysis, and hence nominally identified as the free-surface mode) switch to a different branch at high k. This occurs precisely at the same Γ and k for both c_r and c_i. It turns out that this high-k branch corresponds to the liquid-solid mode, as demonstrated in Figs. 6 and 7. These figures show again that, for $\Gamma<4.89$, the mode corresponding to the liquid-solid interface is destabilized at finite k as Γ is increased from zero, and at high enough values of k, all these curves approach each other. This is again because of the localization of the velocity perturbations near the liquid-solid interface at high k. However, for $\Gamma\sim4.89$ and higher, what starts out at low k as a liquid-solid mode approaches the high-k behavior corresponding to the free-surface mode. Our

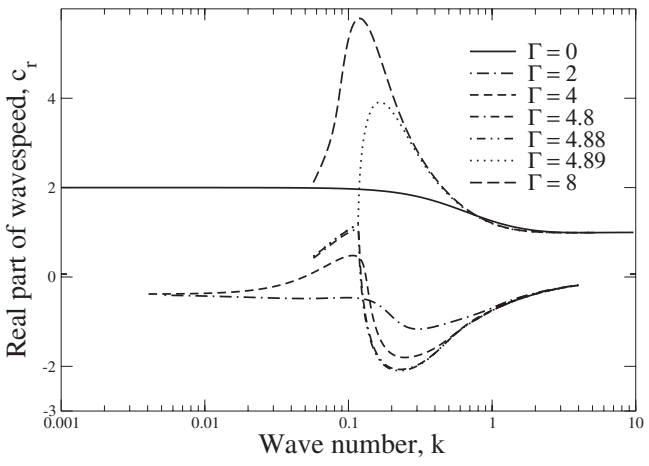

FIG. 7. Behavior of mode 2 plotted in terms of c_r vs k for increasing values of solid deformability parameter Γ: Mode mixing illustrated for $\beta=50°$, Re=0, $\beta=0$, $W=0.5$, $H=1$, $\Sigma_f=2$, $\Sigma_i=1$ (parameters same as in Fig. 4).

results further show that at a particular value of Γ close to 4.89, the eigenvalues corresponding to the two interfacial modes are exactly equal.

This phenomenon, whereby a solution exhibits the low-k behavior corresponding to a given interfacial mode and smoothly crosses over to the high-k behavior of the other interfacial mode, has been referred to as "mode mixing" in the literature, and has been observed in contexts quite different from the problem studied in this paper. For instance, it has been observed in the spectrum of capillary waves and dilatational fluctuations at a *single* liquid surface [48,49], as well as in *two-layer* Bernard-Marangoni instabilities [50,51]. In this study, we observe this mode-mixing phenomenon between modes corresponding to liquid-gas and liquid-solid interfaces. A similar phenomenon was also found to occur for Newtonian liquid film flow past a deformable solid [21]. We find mode mixing between the two interfacial modes to be a robust phenomenon, and it persists for a variety of parametric regimes probed by our numerical analysis. This behavior implies that the clear mode separation that exists for lower values of Γ is no longer true at higher values of Γ, where the dynamics of both the interfaces are highly coupled and hence the two interfacial modes strongly interact with each other. Furthermore, the labeling of the two modes as free surface and liquid solid also becomes a little arbitrary, since it would depend on whether one characterizes a given mode using the low-k or high-k behavior. In the following discussion, to avoid ambiguity, we simply refer to the two modes as mode 1 and mode 2, where modes 1 and 2 refer to the eigenvalues that, respectively, have low-k behavior appropriate to the free surface and liquid-solid interface. However, since our primary interest is in identifying the presence or absence of instabilities, and in the construction of neutral stability diagrams demarcating stable and unstable zones, the mode-mixing phenomenon has little practical relevance for our objectives.

C. Neutral stability diagrams

The important conclusion from the foregoing discussion is that as Γ is increased beyond the critical value given in Eq. (57), the low-wave-number free-surface instability is suppressed at all wave numbers. However, as Γ is increased further, a finite-wave-number instability occurs when the solid becomes sufficiently deformable. We now construct neutral stability diagrams in the Γ-k plane to examine if there is a sufficient range in the values of Γ where there is no instability at any wave number, and present such diagrams for a few representative parameter regimes. These diagrams could be potentially useful in future experimental studies to test the predictions of this work.

We first discuss results for the case of $\beta=0$ in the Oldroyd-B model, which represents the case of pure polymer and no solvent. Figure 8 shows a typical neutral stability diagram demarcating the stable and unstable zones of the different modes. As Γ is increased from very small values, there is a transition from unstable to stable regions for the free-surface mode. There is a range of values of Γ where there is no instability for any wave number; this conclusion

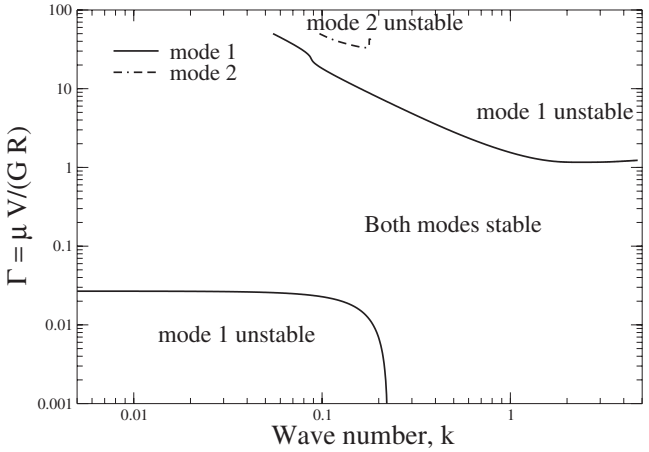

FIG. 8. Neutral stability curves in the Γ-k plane illustrating the presence of a stability window where all modes are stable: Data for the UCM fluid with Re=0, W=0.5, β=0, θ=50°, H=1, Σ_f=2, Σ_i=1.

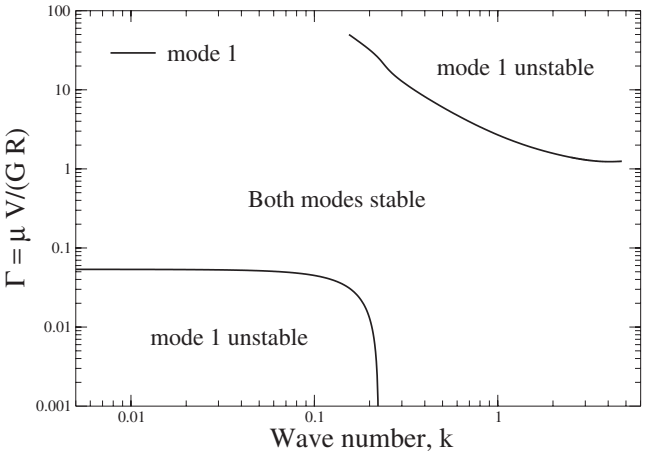

FIG. 10. Neutral stability diagram in the Γ-k plane showing that one of the upper neutral curves is absent as H is decreased to 0.5: Data for a UCM fluid with Re=0, W=0.5, β=0, θ=50°, Σ_f=2, Σ_i=1.

was further corroborated using the spectral method by scanning a range of wave numbers for the possibility of unstable modes, and none were found for this range of Γ. For Γ>1, however, we find an unstable mode at moderate and high values of k, and this mode is due to the first-normal-stress difference at the liquid-solid interface [30,40]. As Γ is increased even further, the free surface itself becomes unstable at finite wave numbers due to wall deformability. The evolution of stable and unstable modes as Γ is increased (for a given value of k) can further be illustrated using the result from the spectral method, as shown in Fig. 9. The eigenspectrum clearly shows how the free-surface mode is stabilized as Γ is increased, and how new unstable modes appear at very high values of Γ for the given value of k. Our numerical results based on the neutral stability diagram show that, as W is increased from 0.5 in Fig. 8 to higher values, the window of Γ where there is no instability decreases with increase in W. However, as H is decreased to 0.5, the stability window in terms of range of Γ increases as shown in Fig. 10. Indeed, our numerical results for this data set show that there is only one unstable mode at high values of Γ, unlike Fig. 8 for H =1. While these two figures displayed data for θ=50°, Fig. 11 shows that similar features prevail even for the vertically inclined case.

We next turn to the case of finite β, i.e., polymer solutions. Figure 12 illustrates that the predictions of instability suppression, and the presence of a stability window where no unstable modes are present, hold for the Oldroyd-B case as well. However, as W is increased to higher values in Fig. 13, we find an island of unstable modes at $k \sim 1$, whose size was found to increase with increase in W, and this rules out the

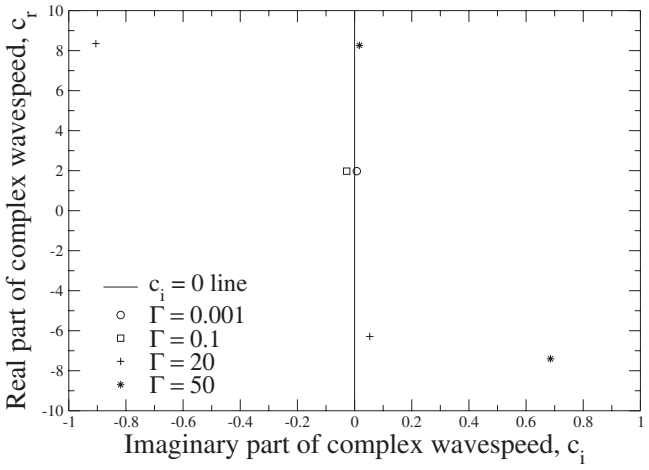

FIG. 9. Eigenvalue spectrum in the c_r-c_i plane for the UCM fluid illustrating the changes in the spectrum as solid deformability Γ is varied. In this plot, the ranges for c_r and c_i are chosen so that the transition from stable to unstable regions is clearly depicted. There are a number of stable modes to the left of the c_i=0 line which are not shown owing to the large magnitudes of c_r and c_i. Data for k=0.1, Re=0, W=0.5, β=0, θ=50°, H=1, Σ_f=2, Σ_i=1.

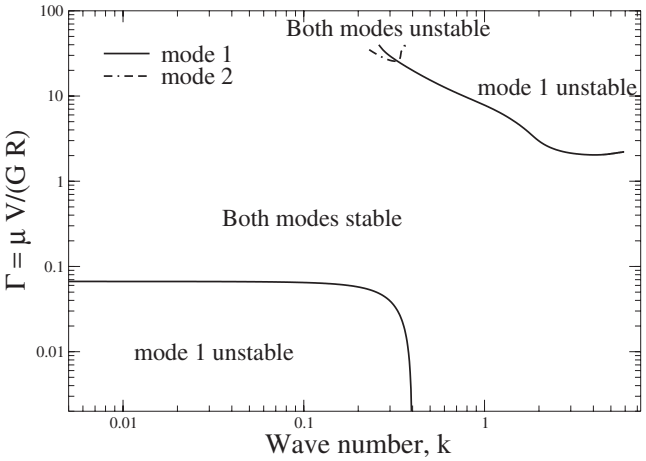

FIG. 11. Neutral stability curves in the Γ-k plane for the vertical configuration, again demonstrating a zone of stability where all the modes are stable: Data for UCM fluid with Re=0, W=0.1, β=0, θ=90°, H=0.5, Σ_f=2, Σ_i=1.

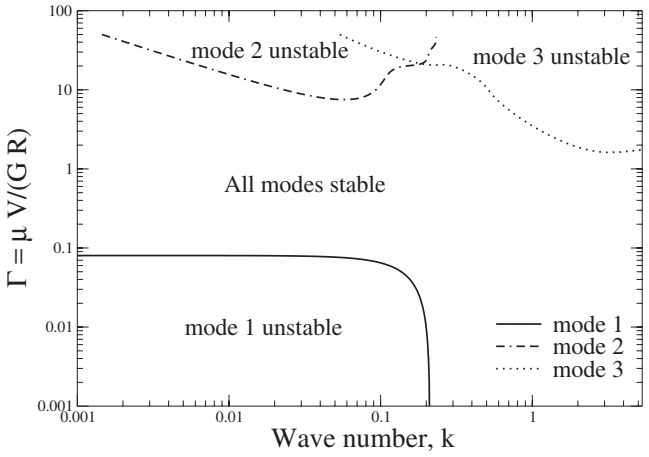

FIG. 12. Neutral stability curves in the Γ-k plane showing that suppression of instabilities applies even for the Oldroyd-B fluid with Re=0.1, W=1, β=0.5, θ=50°, H=0.5, Σ_f=2, Σ_i=1.

possibility of instability suppression at all wave numbers in a polymer solution at higher W. Thus far, the results presented contained only two modes corresponding to the free surface and the liquid-solid interface, and these two modes are stabilized or destabilized as Γ is varied. However, apart from these purely interfacial modes, the coupled fluid-solid problem also admits several other solutions which have been studied well in the literature [34,35]; these modes correspond to free shear waves in a solid, which are modified and destabilized by the liquid flow in the presence of inertia, and hence it is convenient to refer these modes as inertial modes. For the Oldroyd-B fluid at finite inertia, we find these inertial modes being destabilized in the film flow as well, and this is shown in Fig. 14 for θ=90°, where we find additional neutral curves predicted by the spectral method. We have verified that these unstable modes vanish as Re is decreased, and hence belong to the class of inertial modes discussed above. For this parameter set, these additional modes are of no consequence, since they occur at very high values of Γ, and for such high values of Γ, the two interfacial modes themselves are already destabilized. However, for the parameter set shown in Fig. 15, which is at somewhat higher Re=5 and H=5, we find a profusion of unstable modes even at lower value of Γ. The complexity of this neutral stability diagram further underscores the importance of using spectral methods in order to demonstrate the phenomenon of instability suppression. The use of an orthonormal shooting coupled with a Newton-Raphson iteration clearly cannot resolve this complex stability behavior owing to the lack of accurate initial guesses for the various modes. The general trend from our numerical results indicates that, as Re or H is increased, the window of stability (in terms of values of Γ) where no unstable modes are present vanishes eventually. For smaller values of $H \leq 1$, however, it is possible to obtain a range of values of shear modulus where there is no instability at any wave number.

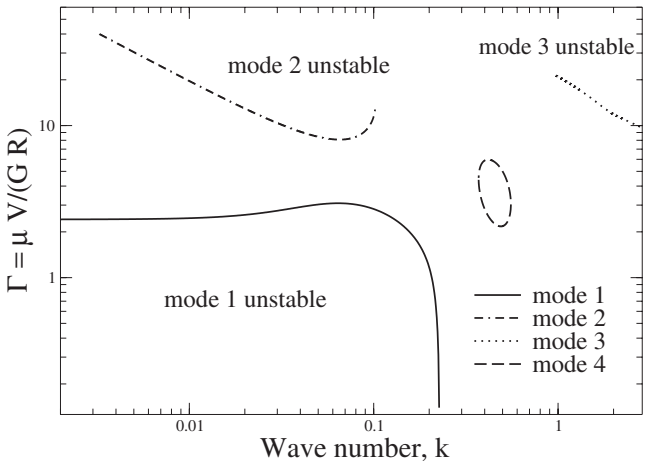

FIG. 13. Neutral stability diagram in the Γ-k plane showing the presence of a new island of unstable modes as W is increased: Data for the Oldroyd-B fluid with Re=0.1, W=8, β=0.5, θ=50°, H=0.5, Σ_f=2, Σ_i=1.

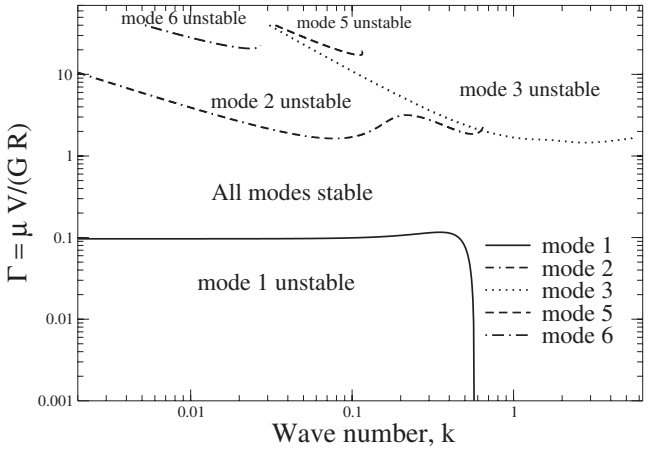

FIG. 14. Neutral stability curves in the Γ-k plane for the vertical geometry: Data for the Oldroyd-B fluid show that new unstable modes appear at higher values of Γ, with Re=0.1, W=0.5, β=0.5, θ=90°, H=1, Σ_f=2, Σ_i=1.

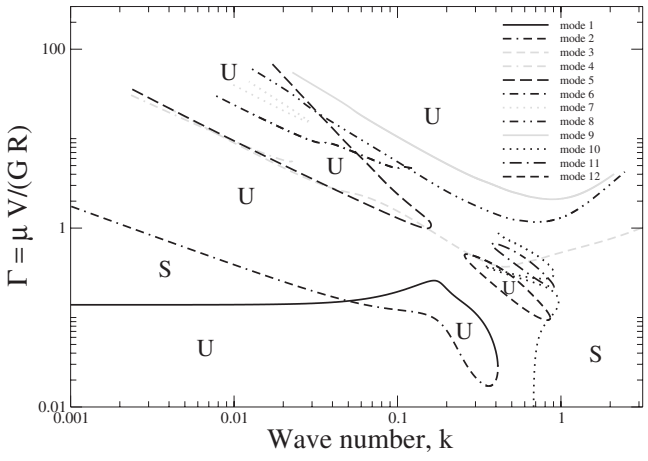

FIG. 15. Neutral stability curves in the Γ-k plane for the inclined geometry: Data for the Oldroyd-B fluid show that new unstable modes proliferate. Re=5, W=1, β=0.5, θ=50°, H=5, Σ_f=2, Σ_i=1. The letters U and S, respectively, denote unstable and stable regions.

V. CONCLUSIONS

The stability of viscoelastic film flow down an inclined plane lined with a deformable solid layer was analyzed using a long-wave asymptotic analysis and a spectral Chebyshev-Tau numerical method. Our primary objective was to determine the effect of deformability of the solid layer on the free-surface unstable mode and other modes present in the composite system. For rigid inclines, viscoelastic film flows are unstable even in the absence of fluid inertia due to fluid elasticity characterized by the Weissenberg number W. Our low-wave-number asymptotic analysis shows that, in the presence of the deformable solid layer, the leading-order wave speed remains real and identical to that for rigid surfaces, and the solid deformability appears at $O(k)$, the same order at which the destabilizing terms due to fluid elasticity and inertia occur. Importantly, the deformability of the solid has a stabilizing effect, and the free-surface instability is suppressed in the limit of low k when the solid deformability parameter Γ increases beyond a threshold value. At finite wave numbers, our numerical solution indicates that the free-surface and liquid-solid interfacial modes can be destabilized at higher values of deformability, but there remains a window of shear modulus of the solid layer where all the modes are stable at all wave numbers. For low values of solid deformability Γ, the interfacial modes corresponding to the two interfaces can be unambiguously distinguished based on their low-k and high-k behavior, but at higher values of Γ, due to mixing of the two interfacial modes, there is a smooth crossover from the low-k behavior of a given mode to the high-k behavior of the second mode. The importance of using a spectral code to demonstrate instability suppression was further exemplified in the results for an Oldroyd-B fluid, where a profusion of unstable modes were shown to appear due to the coupling between shear waves in the solid and the liquid flow, which would not be predicted otherwise. Our results show that solid deformability parameter $\Gamma \sim \rho g R/G$ must be $O(0.01-0.1)$ in order to achieve instability suppression, which suggests that the present predictions can be realized experimentally for polymeric film flows of thickness $\sim 0.1-1$ cm past soft elastic solids of similar thickness with shear modulus $G \sim 1-10$ kPa. Finally, two general conclusions emerge from the present study about film flows past a deformable solid. First, in the low-wave-number limit, the stabilizing contribution due to the solid layer is insensitive to the rheological descriptions used for the liquid and solid layers. Second, even at finite wave numbers, the prediction of the presence of a stable window of shear modulus where all the unstable modes are suppressed is quite general, irrespective of whether the liquid is Newtonian or not, and whether the solid is described by a simple linear elastic model or by a more accurate neo-Hookean model. Thus, our results suggest that the suppression of free-surface instability is likely to be a generic phenomenon in liquid film flows past a deformable solid layer.

[1] T. B. Benjamin, J. Fluid Mech. **2**, 554 (1957).
[2] C.-S. Yih, Phys. Fluids **6**, 321 (1963).
[3] V. Y. Shkadov, Izv. Akad. Nauk SSSR, Mekh. Zhidk. Gaza **1**, 43 (1967).
[4] A. S. Gupta, J. Fluid Mech. **28**, 17 (1967).
[5] A. S. Gupta and L. Rai, Proc. Cambridge Philos. Soc. **33**, 87 (1967).
[6] W. Lai, Phys. Fluids **10**, 844 (1967).
[7] E. S. G. Shaqfeh, R. G. Larson, and G. H. Fredrickson, J. Non-Newtonian Fluid Mech. **31**, 87 (1989).
[8] H.-C. Chang and E. A. Demekhin, *Complex Wave Dynamics on Thin Films* (Elsevier, Amsterdam, 2002).
[9] S. J. Weinstein and K. J. Ruschak, Annu. Rev. Fluid Mech. **36**, 29 (2004).
[10] S. P. Lin, J. N. Chen, and D. R. Woods, Phys. Fluids **8**, 3247 (1996).
[11] S. P. Lin and W. Y. Jiang, Phys. Fluids **14**, 4088 (2002).
[12] W. Y. Jiang and S. P. Lin, Phys. Fluids **17**, 054105 (2005).
[13] C.-T. Huang and B. Khomami, J. Fluid Mech. **425**, 213 (2000).
[14] C.-T. Huang and B. Khomami, J. Non-Newtonian Fluid Mech. **97**, 67 (2001).
[15] E. A. Demekhin, S. Kalliadasis, and M. G. Velarde, Phys. Fluids **18**, 042111 (2006).
[16] M. G. Blyth and C. Pozrikidis, J. Fluid Mech. **521**, 241 (2004).
[17] V. Ya. Shkadov, M. G. Velarde, and V. P. Shkadova, Phys. Rev. E **69**, 056310 (2004).
[18] H.-H. Wei, Phys. Fluids **17**, 012103 (2005).
[19] H.-H. Wei, Phys. Rev. E **71**, 066306 (2005).
[20] V. Shankar and A. K. Sahu, Phys. Rev. E **73**, 016301 (2006).
[21] Gaurav and V. Shankar, Phys. Fluids **19**, 024105 (2007).
[22] C.-T. Huang and B. Khomami, Rheol. Acta **40**, 467 (2001).
[23] T. W. Kao, J. Fluid Mech. **33**, 561 (1968).
[24] D. S. Loewenherz and C. J. Lawrence, Phys. Fluids A **1**, 1686 (1989).
[25] K. P. Chen, Phys. Fluids A **5**, 3038 (1993).
[26] W. Y. Jiang, B. Helenbrook, and S. P. Lin, Phys. Fluids **16**, 652 (2004).
[27] K. P. Chen, J. Non-Newtonian Fluid Mech. **45**, 21 (1992).
[28] V. Kumaran, G. H. Fredrickson, and P. Pincus, J. Phys. II **4**, 893 (1994).
[29] V. Kumaran and R. Muralikrishnan, Phys. Rev. Lett. **84**, 3310 (2000).
[30] V. Gkanis and S. Kumar, Phys. Fluids **15**, 2864 (2003).
[31] M. D. Eggert and S. Kumar, J. Colloid Interface Sci. **278**, 234 (2004).
[32] D. Halpern and J. B. Grotberg, J. Fluid Mech. **244**, 615 (1992).
[33] M. Gad-el hak, in *Proceedings of the IUTAM Symposium on Flow Past Highly Compliant Boundaries and in Collapsible Tubes*, edited by P. W. Carpenter and T. J. Pedley (Kluwer Academic, Dordrecht, 2003), Chap. 9, pp. 191–229.
[34] V. Shankar and V. Kumaran, Eur. Phys. J. B **19**, 607 (2001).

[35] V. Shankar and V. Kumaran, Phys. Fluids **14**, 2324 (2002).
[36] S. A. Orszag, J. Fluid Mech. **50**, 689 (1971).
[37] D. Gottlieb and S. A. Orszag, *Numerical Analysis of Spectral Methods* (SIAM, Philadelphia, 1977).
[38] R. B. Bird, R. C. Armstrong, and O. Hassager, *Dynamics of Polymeric Liquids, Vol. 1: Fluid Mechanics* (John Wiley, New York, 1977).
[39] R. G. Larson, *Constitutive Equations for Polymer Melts and Solutions* (Butterworths, Boston, 1988).
[40] V. Gkanis and S. Kumar, Phys. Fluids **18**, 044103 (2006).
[41] L. E. Malvern, *Introduction to the Mechanics of a Continuous Medium* (Prentice-Hall, Englewood Cliffs, NJ, 1969).
[42] G. A. Holzapfel, *Nonlinear Solid Mechanics* (John Wiley, Chichester, U.K., 2000).
[43] C. Macosko, *Rheology: Principles, Measurements, and Applications* (VCH, New York, 1994).
[44] P. Drazin and W. Reid, *Hydrodynamic Stability* (Cambridge University Press, Cambridge, U.K., 1981).
[45] V. Shankar and V. Kumaran, J. Fluid Mech. **395**, 211 (1999).
[46] D. R. Gardner, S. A. Trogdon, and R. W. Douglass, J. Comput. Phys. **80**, 137 (1989).
[47] H. J. Wilson, M. Renardy, and Y. Renardy, J. Non-Newtonian Fluid Mech. **80**, 251 (1999).
[48] J. C. Earnshaw and A. C. McLaughlin, Proc. R. Soc. London, Ser. A **433**, 663 (1991).
[49] J. C. Earnshaw and A. C. McLaughlin, Proc. R. Soc. London, Ser. A **440**, 519 (1993).
[50] A. Y. Rednikov, P. Colinet, M. G. Velarde, and J. C. Legros, Phys. Rev. E **57**, 2872 (1998).
[51] A. Y. Rednikov, P. Colinet, M. G. Velarde, and J. C. Legros, J. Fluid Mech. **405**, 57 (2000).